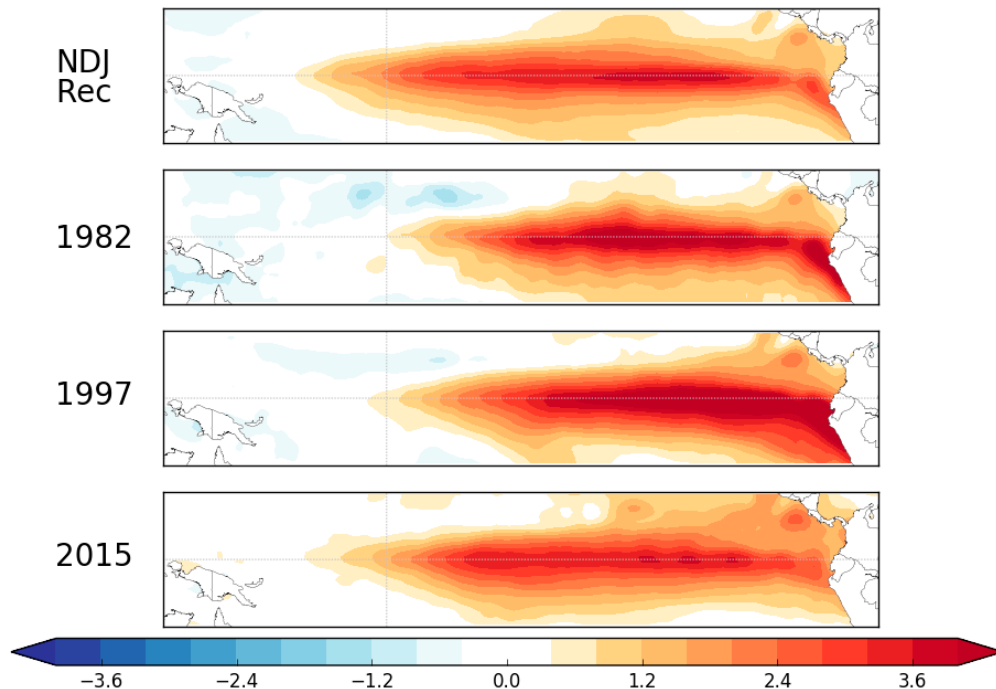


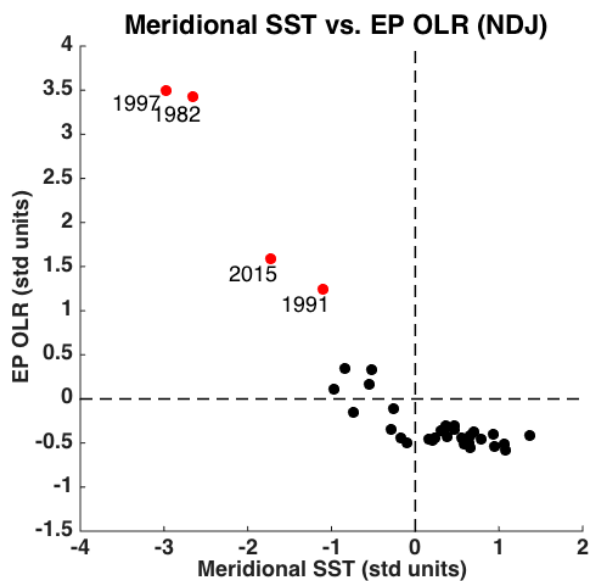
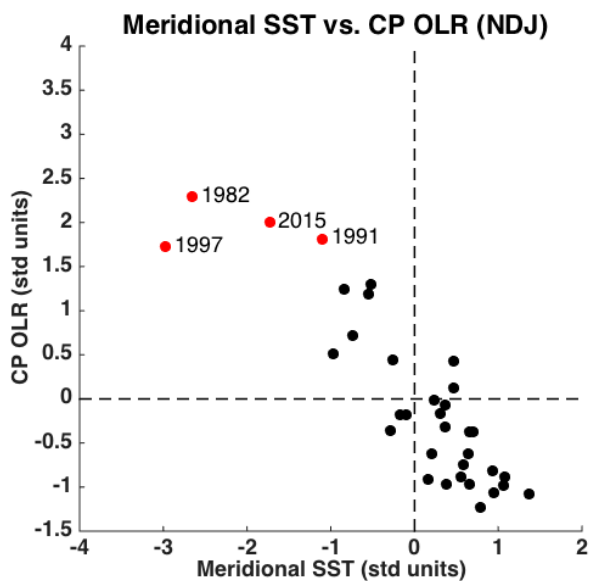
# OBSERVING AND PREDICTING THE 2015/16 EL NIÑO

MICHELLE L. L'HEUREUX, KEN TAKAHASHI, ANDREW B. WATKINS, ANTHONY G. BARNSTON, EMILY J. BECKER, TOM E. DI LIBERTO, FELICITY GAMBLE, JON GOTTSCHALCK, MICHAEL S. HALPERT, BOYIN HUANG, KOBİ MOSQUERA-VÁSQUEZ, AND ANDREW T. WITTENBERG

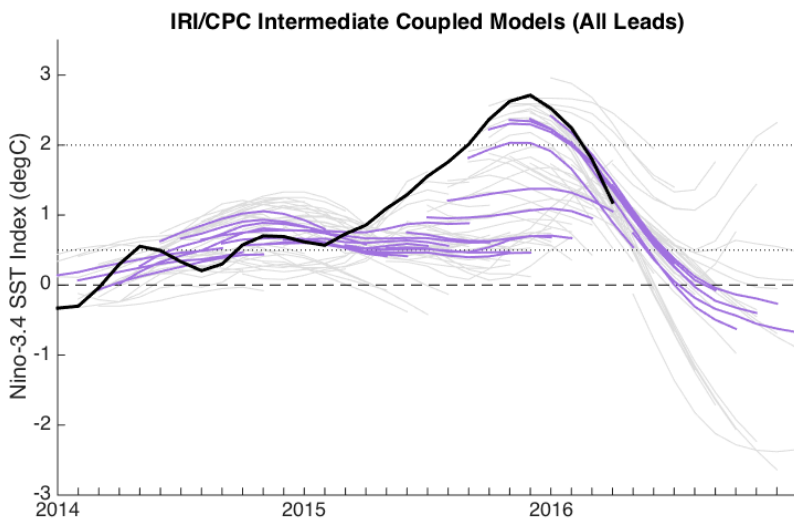
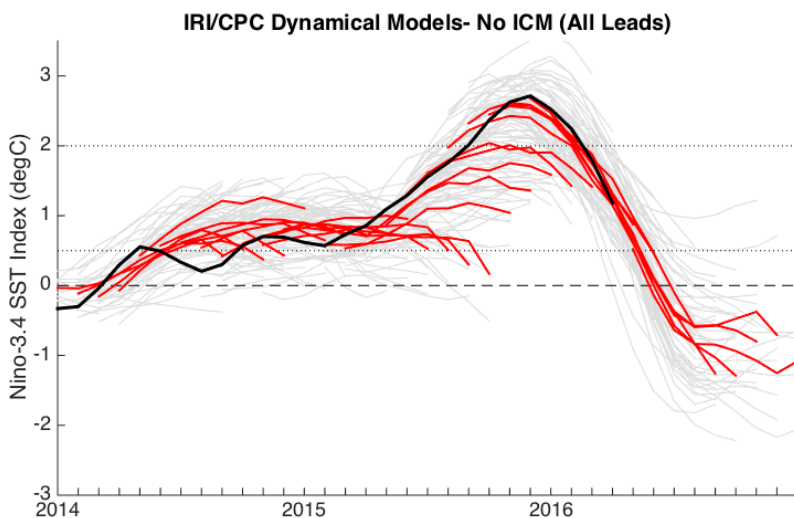
This document is a supplement to “Observing and Predicting the 2015/16 El Niño,” by Michelle L. L’Heureux, Ken Takahashi, Andrew B. Watkins, Anthony G. Barnston, Emily J. Becker, Tom E. Di Liberto, Felicity Gamble, Jon Gottschalck, Michael S. Halpert, Boyin Huang, Kobi Mosquera-Vásquez, and Andrew T. Wittenberg (*Bull. Amer. Meteor. Soc.*, **98**, 1363–1382) • ©2017 American Meteorological Society • Corresponding author: Michelle L’Heureux, michelle.lheureux@noaa.gov • DOI:10.1175/BAMS-D-16-0009.2



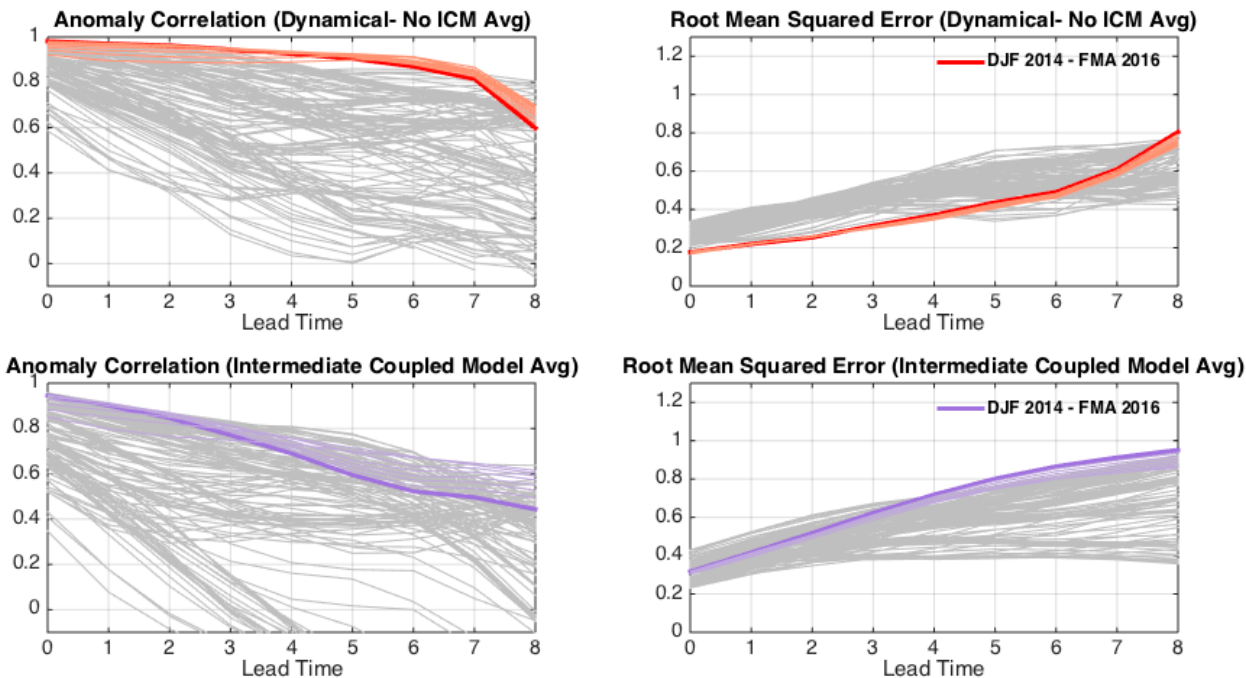
**FIG. ES1.** Reconstruction of (top) Nov–Jan (NDJ) SST anomalies (weighted regression of SST anomalies onto Niño-3.4 index) and (top middle) observed SST anomalies from NDJ 1982/83, (bottom middle) NDJ 1997/98, and (bottom) NDJ 2015/16. Departures are formed by removing monthly means during 1981–2010. Data are based on weekly OISSTv2.



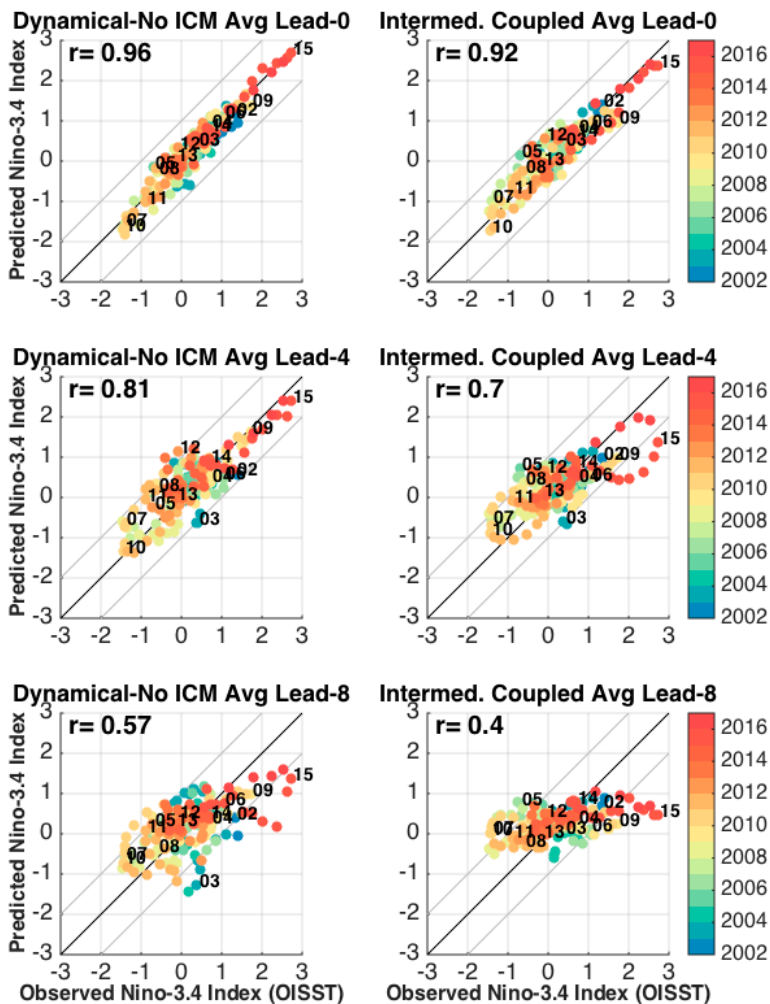
▲ FIG. ES2. Scatterplots of the Nov–Jan standardized meridional SST index values (along the abscissa) against the standardized (left) CP and (right) EP OLR indices (along the ordinate). Each dot represents a single year (Nov–Jan) between 1982 and 2016 with the four most negative meridional SST index values featured in red. The meridional SST index is computed by using the average of the SST anomaly in the region north of the equator ( $5^{\circ}$ – $10^{\circ}$ N,  $150^{\circ}$ – $90^{\circ}$ W) minus the equator ( $2.5^{\circ}$ S– $2.5^{\circ}$ N,  $150^{\circ}$ – $90^{\circ}$ W).



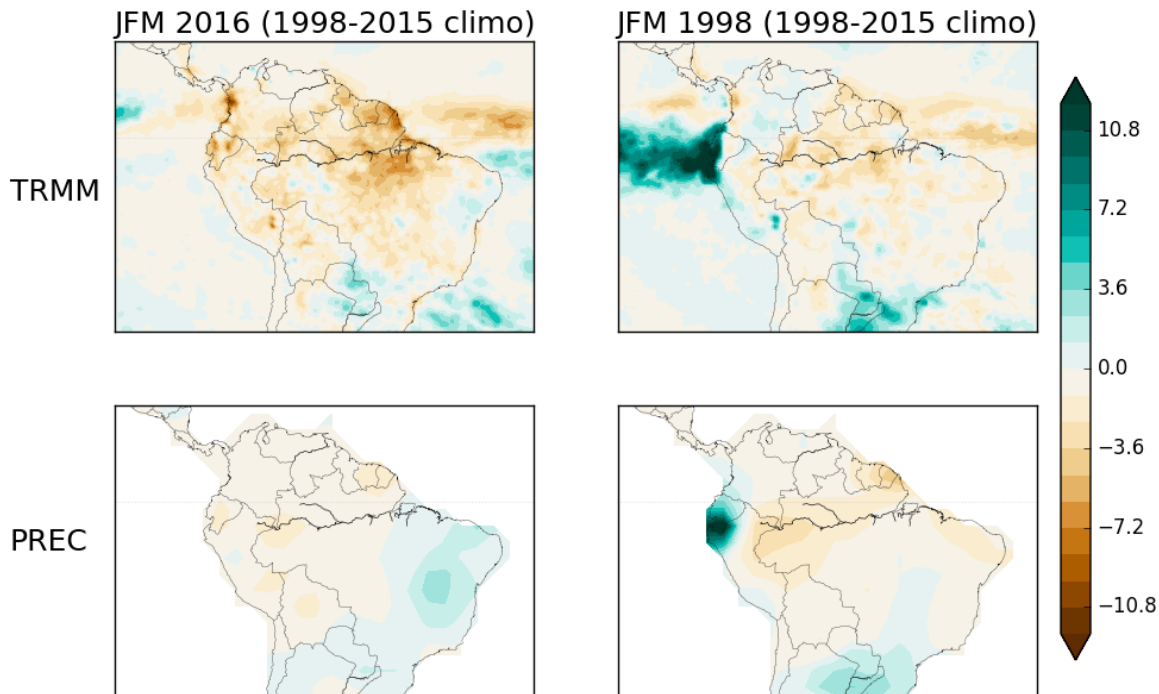
◀ FIG. ES3. As in Fig. 7 in main paper, but showing the multimodel average of the dynamical models (top) without the intermediate coupled models (ICMs) included and (bottom) the multimodel average of only the ICMs.



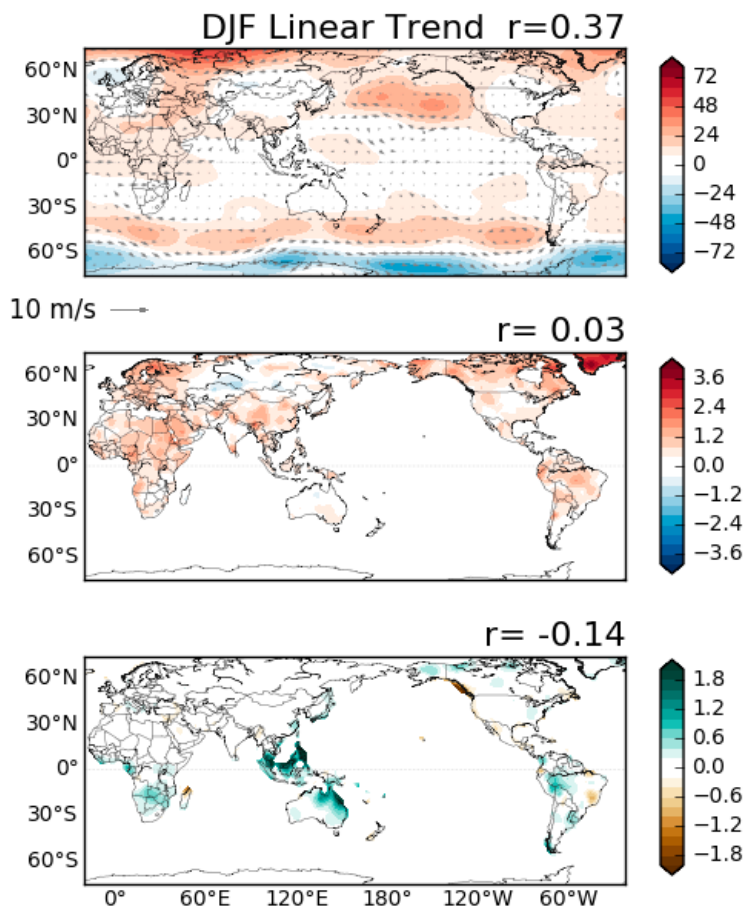
▲ FIG. ES4. As in Fig. 8 in main paper, but showing the correlation and root-mean-square error of the multimodel average of the dynamical models (top) without the ICMs included and (bottom) the multimodel average of only the ICMs.



► FIG. ES5. As in Fig. 9 in main paper, but showing scatterplots based on (left) the dynamical models without the ICMs included and (right) the multimodel average of only the ICMs.



▲ FIG. ES6. Jan–Mar (JFM) precipitation anomalies for (left) 2016 and (right) 1998 from (top) the  $0.25^\circ \times 0.25^\circ$  gridded Tropical Rainfall Measuring Mission (TRMM) satellite data and (bottom) the gauge-based Precipitation Reconstruction Dataset (PREC)  $2.5^\circ \times 2.5^\circ$  gridded dataset. Historically, TRMM is one of the datasets relied upon in this region because of the lack of dense station coverage. Departures are formed by removing monthly means during 1998–2015 (TRMM began in 1998).



► FIG. ES7. As in Fig. 10 in main paper, but showing the anomalies formed from the least-squares linear fit across Dec–Feb (DJF) averages over the period 1979–2015 (excluding DJF 2015/16). The  $r$  values show the spatial correlation coefficient between the observational and trend anomalies.